Linearization of the Closed-Loop Dynamics of a Dual-Spin Spacecraft

KEVIN J. PHILLIPS*
RCA Corporation, Princeton, N. J.

A dual-spin spacecraft consists of a despun platform and a motor-coupled spinning member. Spin axis position control of the platform is achieved by closed-loop momentum interchange between the two bodies. A major control problem is the cross-coupling of the three axes dynamics, which under the influence of position control can lead to nutation buildup in an otherwise stable spacecraft. This paper derives a linearized transfer function from the dynamics, and demonstrates its use in a simple technique which can readily determine spacecraft nutational stability and its margins under the influence of the closed-loop control. The technique was used for the analysis of the ITOS-1 spacecraft and an example of a typical set of results is presented. These results illustrate the transition from stable to unstable spacecraft performance as selected parameters are varied and demonstrate how a clear insight into destabilizing parametric trends becomes readily apparent. The results are compared with equivalent results derived from a fully nonlinear, hybrid-computer simulation of the ITOS-1 spacecraft. The comparison provides very good correlation between the two sets of results, indicating the high degree of precision with which the linearization technique is capable of predicting stable operation.

Nomenclature

I_{11},I_{22},I_{33} = spacecraft moments of inertia about the center of mass with respect to yaw, roll, and pitch axes
I_{12},I_{13},I_{23} = products of inertia associated with those axes
I_f = pitch wheel moment of inertia about the spin (pitch) axis
I_p = pitch moment of inertia of the platform without the wheel $= I_{33} - I_f$
I_D = moment of inertia of the moving mass of the viscous nutation damper with respect to the roll axis
$\omega_1,\omega_2,\omega_3$ = angular velocities about the yaw roll and pitch axes
H = spacecraft total angular momentum
H_1,H_2,H_3 = spacecraft angular momentum about yaw roll and pitch axes
ω_f = absolute angular velocity of wheel
ω_{fr} = angular velocity of wheel relative to platform
ω_D = angular velocity of viscous nutation damper relative to platform
ω_o = orbital rate
T = motor accelerating torque (positive for wheel acceleration)
γ = damper torque constant in torque per unit relative angular velocity
ϕ = spacecraft roll angle, defined as the angle between the pitch axis and the plane formed by the orbit normal and velocity vector
ψ = spacecraft yaw angle, defined as the angle between the orbit normal and the plane formed by the pitch axis and local vertical
θ_p = spacecraft pitch error, defined as the angle between the yaw axis and the plane formed by the pitch axis and the local vertical
α = constant angle between line of sight of the rotating horizon scanner and the positive pitch axis
β = pitch angle measured by the rotating horizon scanner mounted on the wheel, between the point of intercept of the sky-Earth Horizon, and the plane formed by the pitch axis and local vertical
β_o = value of β at a roll angle of zero
θ_E = pitch error sensed by the horizon scanner
μ = half-angle of Earth as seen by the spacecraft
θ_N = half cone angle of nutation cycle
$M(s)$ = transfer function of the open pitch control loop without dynamic cross-coupling
ω_N = nutation frequency $= 1/T_D$

Presented as Paper 70-975 at the AIAA Guidance, Control and Flight Mechanics Conference, Santa Barbara, Calif., August 17–19, 1970; submitted August 19, 1970; revision received March 29, 1971. Work described in this paper was supported by the NASA Goddard Space Flight Center under Contract NAS5-10306.

* Astro-Electronics Division.

Introduction

THE dual-spin spacecraft is an Earth orbiting device consisting of a despun platform which is generally Earth-oriented, and a rotating member (or wheel) coupled by a motor drive. Earth orientation is achieved about the spin axis by means of a momentum interchange between the spinning and despun members. The angular error that the platform has about the spin axis relative to some desired reference is sensed, and by closed-loop control this error is used to drive the motor in such a direction as to reduce the error toward zero.

A major problem associated with this type of system is the cross-coupling of the dynamics of the spin axis with the two transverse axes. If the spin axis is not exactly a principal axis, a torque from the motor will not only act to change the relative speed between the platform and wheel, but will also induce angular rates about the other axes. These transverse rates manifest themselves as nutation of the spin axis about the total momentum vector. There are many examples in the literature[1,2,3] which show that, provided the spacecraft momentum and inertia distributions obey certain basic criteria, in the absence of any further motor disturbing torques, this nutation can be forced to decay by means of an energy dissipating damper on either of the transverse axes. However, because the nutation motion can cause a cyclic variation of the angular error sensed by the closed-loop control, this sensed error will in turn demand a cyclic variation of motor torque at the nutation frequency. Since particular values of the phase and gain of the control loop could reinforce the build up of nutation, with a subsequent instability the control-loop parameters must be chosen carefully.

The original method chosen to determine the closed-loop performance of the ITOS-1 spacecraft, under its various

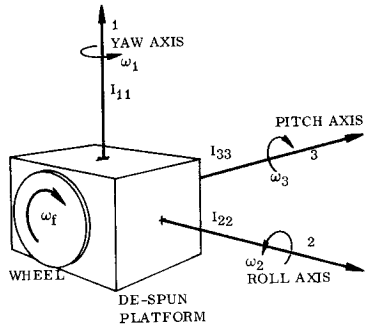

Fig. 1 Spacecraft conventions.

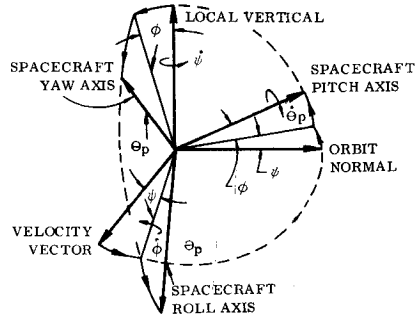

Fig. 2 Inertial conventions.

initial conditions and tolerances, was to make a full nonlinear simulation on a hybrid computer. Time responses of the system were obtained, from which the stability was gauged by measuring the time constant of the decay or increase of the nutation angle. This simulation showed that not only was stability critically dependent upon the moments and products of inertia, the angular momentum, the roll angle, the pitch sensor scan angle, the damper effectiveness, and all of the motor control-loop parameters, but the cross-coupling was such that changes within the tolerance boundaries of certain parameters could reverse the worst-case tolerance extremes of the other parameters. This made establishment of the overall worst cases for the various spacecraft operating modes very time consuming and difficult. It was therefore decided to attempt to linearize the seven or more nonlinear differential equations describing the dynamics into a single transfer function that would relate the sensed closed-loop position error to the drive motor accelerating torque. This transfer function could then be used, along with the motor control-loop transfer functions, in one of the standard methods of stability analysis, such as Nyquist or Nichols, in order to make rational predictions of performance.

Description of System

The spacecraft system studied was that of ITOS-1. The body and inertial conventions used are shown in Figs. 1 and 2. The spacecraft has a viscous nutation damper consisting of a hollow closed tube which contains a light oil. The plane of the tube is perpendicular to one of the transverse axes so that nutational cyclic angular body rates about that axis cause longitudinal liquid motions in the tube. The liquid flow results in a frictional energy loss which, because of the law of conservation of momentum, causes the nutational motion to decay. The transverse axis selected is the roll axis, and the equations are written on this basis. However, the transfer function derivation procedure is similar if the damper had been on the yaw axis, and although not proven in this paper, the modification required to the final transfer function for a damper on the yaw axis is indicated at the end of the Sec. entitled "Transfer Function with Fluid Damper."

The spacecraft senses its pitch error for closed-loop control by means of a single horizon sensor mounted on the wheel, the geometry of which is illustrated in Fig. 3. Its line of sight is canted at an angle α from the positive spin axis such that as the wheel spins, the line of sight traces out a cone about the spin axis, whose half-angle is equal to α or $(\pi - \alpha)$ radians. The pitch error, θ_E is determined as the difference between the angular position of the wheel at the sky-Earth horizon crossing and its angular position as a wheel-mounted sensor passes a spacecraft reference point. The reference is arranged to be coincident with the horizon, and hence to give zero sensed pitch error for an orthogonally oriented spacecraft. In algebraic form the sensed pitch error is

$$\theta_E = \theta_p + \beta - \beta_0$$

$$\beta = \cos^{-1}[\tan\phi/\tan\alpha + \cos\mu/\sin\alpha\cos\phi]$$

$$\beta_0 = \cos^{-1}[\cos\mu/\sin\alpha]$$

These expressions show that at zero roll, the sensed pitch error is equal to the true pitch error of θ_p, but at all other roll angles the $\beta - \beta_o$ term represents a further cross-coupling of the roll angle into the sensed pitch error. This coupling is in addition to that which is described in the introduction, and it is due to the way the pitch error is sensed from the curved horizon. The effect of the coupling will be considered here, but for a spacecraft system that is capable of sensing the true pitch error, the effect of the β term can easily be removed from the final form of the transfer function by letting the term $d\beta/d\phi$ become zero.

Linearization of the Dynamical Equations

The equations defining the spacecraft motion are as follows

$$H^2 = H_1^2 + H_2^2 + H_3^2$$

$$I_{11}\dot{\omega}_1 - I_{12}\dot{\omega}_2 - I_{13}\dot{\omega}_3 = H_2\omega_3 - H_3\omega_2 \quad (1)$$

$$-I_{12}\dot{\omega}_1 + I_{22}\dot{\omega}_2 - I_{23}\dot{\omega}_3 + I_D\dot{\omega}_D = H_3\omega_1 - H_1\omega_3 \quad (2)$$

$$-I_{13}\dot{\omega}_1 - I_{23}\dot{\omega}_2 + I_{33}\dot{\omega}_3 + I_f\dot{\omega}_{fr} = H_1\omega_2 - H_2\omega_1 \quad (3)$$

where Eqs. (1-3) are the time derivatives of the following momentum equations in the absence of applied torques:

$$H_1 = I_{11}\omega_1 - I_{12}\omega_2 - I_{13}\omega_3$$

$$H_2 = -I_{12}\omega_1 + I_{22}\omega_2 + I_{23}\omega_3 + I_D\omega_D$$

$$H_3 = -I_{13}\omega_1 - I_{23}\omega_2 + I_{33}\omega_3 + I_f\omega_{fR}$$

$$I_f\dot{\omega}_3 + I_f\dot{\omega}_{fr} = T \quad (4)$$

$$I_D\dot{\omega}_2 + I_D\dot{\omega}_D = -\gamma\omega_D \quad (5)$$

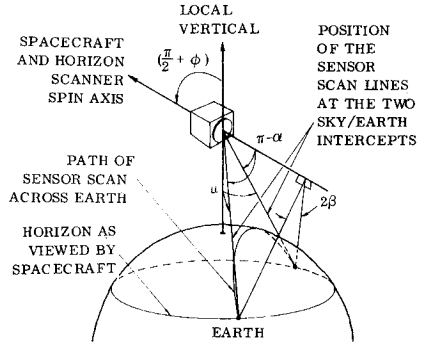

Fig. 3 Geometry of the horizon scanner.

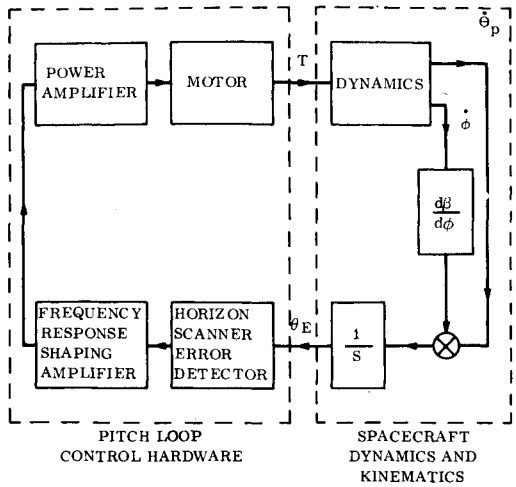

Fig. 4 Block diagram of pitch control loop.

$$\dot{\theta}_p = \omega_3 - \tan\phi(\omega_1 \cos\theta_p - \omega_2 \sin\theta_p) - \omega_0(\cos\phi \cos\psi + \tan\phi \sin\phi \cos\psi) \quad (6)$$

$$\dot{\psi} = (\omega_1 \cos\theta_p - \omega_2 \sin\theta_p + \omega_0 \sin\phi \cos\psi)/\cos\phi \quad (7)$$

$$\dot{\phi} = \omega_1 \sin\theta_p + \omega_2 \cos\theta_p - \omega_0 \sin\psi \quad (8)$$

$$\theta_E = \theta_p + \beta - \beta_0$$

By differentiating with respect to time, this last expression can be written

$$\dot{\theta}_E = \dot{\theta}_p + (d\beta/d\phi)\cdot\dot{\phi} \quad (9)$$

In order to make the necessary linearizations the following assumptions have to be made: θ_p,ϕ are small angles; ω_0 is small compared with the body rates, $\omega_1,\omega_2,\omega_3$; the nutation half cone angle, θ_N is small; and the total spin axis momentum is large compared to the transverse axes' momentum. These assumptions will generally be true for the spacecraft operating in the quiescent state, and they allow the following approximation to be made in the above equations. $H_1 = 0$, $H_2 = 0$, $H_3 = H$ = a constant. $d\beta/d\phi$ is a constant, evaluated at its operating value of α and its average roll angle. Based on these linearizations, the above equations are reduced to the following seven linear differential equations with constant coefficients:

$$I_{11}\dot{\omega}_1 - I_{12}\dot{\omega}_2 - I_{13}\dot{\omega}_3 = -\omega_2 H_3 \quad (10)$$

$$-I_{12}\dot{\omega}_1 + I_{22}\dot{\omega}_2 - I_{23}\dot{\omega}_3 + I_D\dot{\omega}_D = \omega_1 H_3 \quad (11)$$

$$-I_{13}\dot{\omega}_1 - I_{23}\dot{\omega}_2 + (I_{33} - I_f)\dot{\omega}_3 = -T \quad (12)$$

$$I_D\dot{\omega}_D + I_D\dot{\omega}_2 = -\gamma\omega_D \quad (13)$$

$$\dot{\theta}_p = \omega_3 \quad (14)$$

$$\dot{\phi} = \omega_2 \quad (15)$$

$$\dot{\theta}_E = \dot{\theta}_p + (d\beta/d\phi)\dot{\phi} \quad (16)$$

Derivation of the Dynamics Transfer Function

Figure 4 is a simplified block diagram of the pitch control loop. It indicates that, in order to examine the closed-loop stability of the system, the cross-coupled relationship of θ_E to T is required.

An attempt to combine the above equations directly into a transfer function relating θ_E to T would yield a third order polynomial in s in the denominator, which is algebraically unfactorable. Also, the coefficients of the polynominal are of such unwieldy proportions that the transfer function's use in that form would not fulfill the purpose of simplicity. However, a method has been derived of obtaining approximate factors for the polynomial, from which the desired simplified form can be obtained. The method consists of first deriving the degenerate case of the system with no nutation damper, and then introducing the damper equations into the final form.

Transfer Function without Nutation Damper

With no nutation damper, the term $I_D\dot{\omega}_D$ disappears from Eq. (11) and Eq. (13) does not exist. Substituting Eqs. (14) and (15) into Eqs. (10–12) and taking Laplace transforms, gives the following relationship:

$$A\begin{bmatrix}\omega_1\\ \phi\\ \theta_p\end{bmatrix} = \begin{bmatrix}0\\ 0\\ -T\end{bmatrix} \quad (17)$$

where

$$A = \begin{bmatrix} sI_{11} & s(H_3 - sI_{12}) & -s^2I_{13} \\ -(H_3 + sI_{12}) & s^2I_{22} & -s^2I_{23} \\ -sI_{13} & -s^2I_{23} & s^2I_p \end{bmatrix} \quad (18)$$

then the adjoint of $A = B$ where

$$B = \begin{bmatrix} s^4(I_{22}I_p - I_{23}^2) & -s^3(H_3 - sI_{12})I_p + s^4I_{13}I_{23} & -1s^3(H_3 - sI_{12})I_{23} + s^4I_{13}I_{22} \\ s^2(H_3 + sI_{12})I_p + s^3I_{13}I_{23} & s^3I_{11}I_p - I_{13}^2) & s^3I_{11}I_{23} + s^2(H_3 + sI_{12})I_{13} \\ s^2(H_3 + sI_{12})I_{23} + s^3I_{13}I_{22} & s^3I_{11}I_{23} - s^2(H_3 - sI_{12})I_{13} & s^3I_{11}I_{22} + s(H_3^2 - s^2I_{12}^2) \end{bmatrix} \quad (19)$$

The above matrix equation can now be inverted as

$$\begin{bmatrix}\omega_1\\ \phi\\ \theta_p\end{bmatrix} = \frac{B}{\det A}\begin{bmatrix}0\\ 0\\ -T\end{bmatrix} \quad (20)$$

where $\det A$ is the determinant of A and equals:

$$s^3[I_pH_3^2 + s^2(I_{11}I_{22}I_p - I_pI_{12}^2 - I_{22}I_{13}^2 - I_{11}I_{23}^2 - 2I_{13}I_{23}I_{12})] \quad (21)$$

This matrix inversion now yields the following two relationships.

$$\phi/T = -I_{13}\cdot[1 + s(I_{12}/H_3 + I_{11}I_{23}/H_3I_{13})]/(1 + \xi)sI_pH_3 \quad (22)$$

where

$$\xi \equiv (s^2/H_3^2)(I_{11}I_{22} - I_{12}^2 - I_{22}I_{13}^2/I_p - I_{11}I_{23}^2/I_p - 2I_{13}I_{23}I_{12}/I_p) \quad (23)$$

and

$$\theta_p/T = -H_3\cdot[1 + s^2(I_{11}I_{22} - I_{12}^2)/H_3^2]/(1 + \xi)s^2I_pH_3 \quad (24)$$

Now Eq. 16 can be written as

$$s\cdot\theta_E/T = s\cdot\theta_p/T + d\beta/d\phi\cdot\phi/T\cdot s \quad (25)$$

Thus

$$\frac{\theta_E}{T} = \frac{-1}{s^2I_p}\left\{1 + \frac{s}{H_3}I_{13}\frac{d\beta}{d\phi} + \frac{s^2}{H_3^2}\times\left[I_{11}I_{22} - I_{12}^2 + \frac{d\beta}{d\phi}(I_{12}I_{13} + I_{11}I_{23})\right]\right\}\frac{1}{(1 + \xi)} \quad (26)$$

Transfer Function with Fluid Damper

The derivation of Eqs. (22) and (24) was based on the assumption that there was no fluid damper in the system. If the damper is to be considered, Eq. (13) and the term $I_D\dot{\omega}_D$

in Eq. (11) are reintroduced, which on taking Laplace transforms can be written:

$$\omega_D = -sI_D\omega_2/[\gamma(1 + sI_D/\gamma)] \tag{27}$$

and

$$-sI_{12}\omega_1 + sI_{22}\omega_2 - sI_{23}\omega_3 + sI_D\omega_D = \omega_1 H_3 \tag{28}$$

Combining Eqs. (14, 15, 27 and 28) gives:

$$-(H_3 + sI_{12})\omega_1 + s^2 I_{22}\frac{[1 + s(1 - I_D/I_{22})I_D/\gamma]}{(1 + sI_D/\gamma)}\phi - s^2 I_{23}\theta_p = 0$$

Comparing this equation with Eq. (17a) [derived from Eq. (17)]

$$-(H_3 + sI_{12})\omega_1 + s^2 I_{22}\phi - s^2 I_{23}\theta_p = 0 \tag{17a}$$

makes it obvious that the only change that the fluid damper will introduce to the over-all transfer function is to introduce the product term:

$[1 + s(1 - I_D/I_{22})I_D/\gamma]/(1 + sI_D/\gamma)$ wherever I_{22} appears.

Making $a = I_D/\gamma$ and $k = 1 - I_D/I_{22}$, this product term becomes

$$(1 + aks)/(1 + as)$$

Equation (22) can be rewritten as

$$\frac{\phi}{T} = \frac{-1}{s}\cdot\frac{[H_3 I_{13} + s(I_{12}I_{13} + I_{11}I_{23})]}{I_p H_3^2 + s^2[I_{22}(I_{11}I_p - I_{13}^2) - I_{12}^2 I_p - I_{11}I_{23}^2 - 2I_{12}I_{13}I_{23}]} \tag{29}$$

In this expression it can be seen that I_{22} appears only once, and here the above product term should be applied. First, however, the following simplifying substitutions will be made

$$L = I_p H_3^2 \qquad M = I_{22}(I_{11}I_p - I_{13}^2)$$
$$N = I_p I_{12}^2 + I_{11}I_{23}^2 + 2I_{12}I_{13}I_{23} \tag{30}$$

such that

$$\frac{\phi}{T} = \frac{-1}{s}\cdot\frac{[H_3 I_{13} + s(I_{12}I_{13} + I_{11}I_{23})]}{L[1 + s^2(M/L - N/L)]} \tag{31}$$

Thus when the damper correction term is applied, this becomes:

$$\frac{\phi}{T} = \frac{-1}{s}\cdot\frac{[H_3 I_{13} + s(I_{12}I_{13} + I_{11}I_{23})]}{L\{1 + s^2[(M/L)(1 + kas)/(1 + as) - N/L]\}} \tag{32}$$

Expanding this gives:

$$\frac{\phi}{T} = \frac{-[H_3 I_{13} + s(I_{12}I_{13} + I_{11}I_{23})](1 + as)}{sL\{1 + as + [(M - N)/L]s^2 + [a(Mk - N)/L]s^3\}} \tag{33}$$

To help in the factoring of this denominator, we know that if $k = 1$, the fluid damper is removed and so the factors of the denominator must return to that shown in Eq. (31).

That is, we know that

$$1 + as + [(M - N)/L]s^2 + [a(M - N)/L]s^3 = (1 + as)\{1 + [(M - N)/L]s^2\} \tag{34}$$

Therefore, in order to find the factors of the denominator of Eq. (33) when $k \cong 1$, we can let them be

$$[1 + (a + \delta a)s][1 + \delta f s + \{(M - N)/L + \delta e\}s^2] \tag{35}$$

Expanding Eq. (35), ignoring δ products, and equating to the denominator expression, we have:

$$1 + as + [(M - N)/L]s^2 + a[(Mk - N)L]s^3 = 1 + (a + \delta a + \delta f)s + [(M - N)/L + \delta e + a\delta f)s^2 + \{a[(M - N)/L] + \delta a[(M - N)/L] + a\delta e\}s^3 \tag{36}$$

Equating like coefficients:

$$\delta a = -\delta f, \quad \delta e = -a\delta f$$
$$a[(Mk - N)/L] = a(M - N)/L + \delta a(M - N)/L + a\delta e \tag{37}$$

whence

$$\delta a = \frac{aM(k - 1)}{M - N + a^2 L}, \quad \delta f = \frac{-aM(k - 1)}{M - N + a^2 L}, \quad \delta e = \frac{a^2 M(k - 1)}{M - N + a^2 L} \tag{38}$$

Thus

$$a + \delta a = \frac{a(Mk - N + a^2 L)}{M - N + a^2 L}$$
$$\frac{M - N}{L} + \delta e = \frac{(M - N)^2 + a^2 L(Mk - N)}{L(M - N + a^2 L)} \tag{39}$$

Generally it will be true that $N \ll M$ and $k \cong 1$. (For example, the value of k for ITOS-1 is 0.997 and the ratio of M to N is about 10,000, even though this spacecraft has large products of inertia. For vehicles whose control axes are more nearly principal axes, this ratio will be even larger.)

Thus, it is very close to the truth to make $N = Nk$ in the difference term $a^2 L\ (Mk - N)$ in the numerator of Eq. (39). Then

$$\frac{M - N}{L} + \delta e = \frac{M - N}{L}\cdot\frac{(M - N + a^2 kL)}{(M - N + a^2 L)} \tag{40}$$

Therefore, we can now say that the denominator of Eq. (33) factors as follows:

$$sL\left[1 + as + \frac{M - N}{L}s^2 + \frac{a(Mk - N)s^3}{L}\right] = sL\left[1 + \left(\frac{Mk - N + a^2 L}{M - N + a^2 L}\right)as\right]\left[1 + \frac{aM(1 - k)}{M - N + a^2 L}s + \left(\frac{M - N + a^2 kL}{M - N + a^2 L}\right)\cdot\frac{M - N}{L}s^2\right] \tag{41}$$

which reduces to the following form, when k is put equal to 1.

$$sL(1 + as)(1 + (M - N)s^2/L) \tag{42}$$

which, on cancelling the $(1 + as)$ term becomes the same as the original undamped denominator.

In the transfer function, ϕ/T, the numerator $(1 + as)$ can, in fact be cancelled with the denominator single root because the difference is so small that it would not affect the system. The additional product term $(M - N + a^2 kL)/(M - N + a^2 L)$ in the s^2 term was numerically examined and it was found that within any anticipated parameter values and tolerances in the ITOS-1 system, its value would never be further from unity than 0.998. This number, although close to unity, is not close enough to make it obvious that it could be ignored. Therefore we will call the term Q and continue the analysis to see what effect Q may have on the ultimate transfer function of θ_E to T. The principal effect of including the fluid damper in the equations is to introduce the s term into the denominator quadratic function, with a coefficient of

$$aM(1 - k)/(M - N + a^2 L)$$

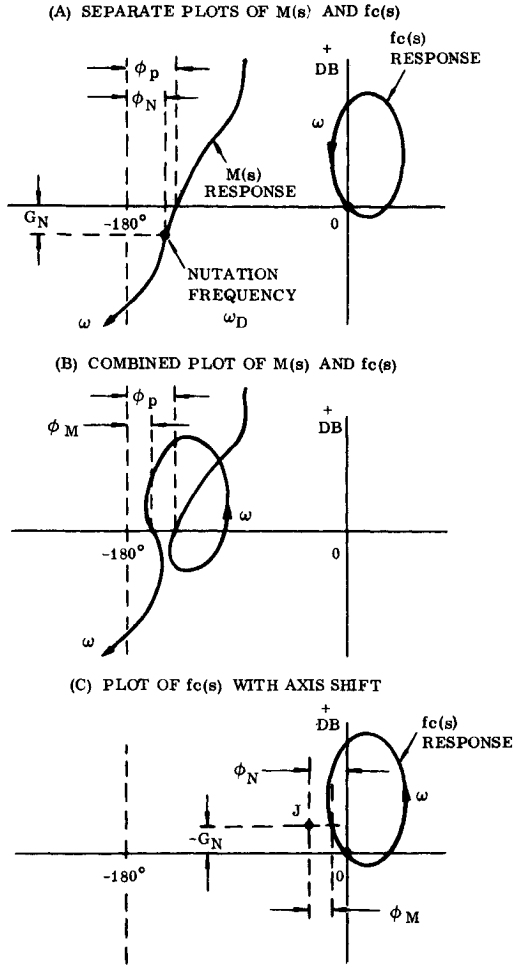

Fig. 5 Typical phase-gain plots.

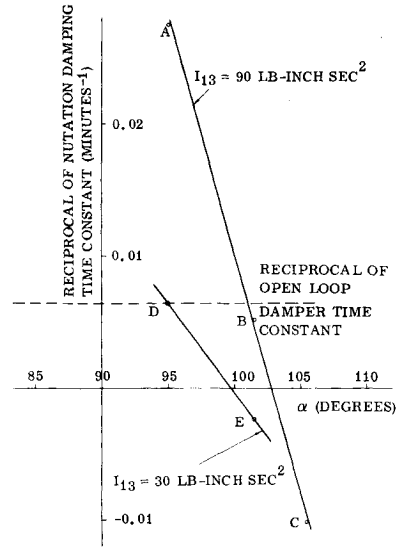

Fig. 6 Reciprocal of nutation damping time constant as a function of α and I_{13}.

Substituting back, this term becomes

$$\frac{I_D/\gamma \cdot I_{22}(I_{11}I_p - I_{13}^2)I_D/I_{22}}{I_{22}(I_{11}I_p - I_{13}^2) - I_{12}^2I_p - I_{11}I_{23}^2 - 2I_{12}I_{13}I_{23} + (I_D^2/\gamma^2)I_pH_3^2} \tag{43}$$

Since this term defines only the degree of damping of the transfer function, no significant error will develop if small approximations are made to it. Thus, ignoring summing terms involving cross products of inertia we have the s coefficient $= I_D^2I_{11}\gamma/(I_{22}I_{11}\gamma^2 + I_D^2H_3^2)$. Thus:

$$\frac{\phi}{T} = \frac{-I_{13}}{sI_pH_3} \cdot \frac{[1 + (s/H_3)(I_{12} + I_{11}I_{23}/I_{13})]}{1 + [I_D^2I_{11}\gamma H_3/(I_{22}I_{11}\gamma^2 + I_D^2H_3^2)](s/H_3) + Q\xi} \tag{44}$$

To derive the relationship of θ_p to T, when the damper is present, each I_{22} in Eq. (24) must be multiplied by $(1 + kas)/(1 + as)$ as before.

$$\frac{\theta_p}{T} = -\frac{1}{s^2I_p} \cdot \frac{[1 + s^2/H_3^2\{I_{11}I_{22}(1 + kas/1 + as) - I_{12}^2\}]}{1 + \{I_{22}[(I_{11} - I_{13}^2)/I_p](1 + kas)/(1 + as) - I_{12}^2 - (I_{11}I_{23}^2 + 2I_{12}I_{23}I_{13})/I_p\}s^2/H_3^2} \tag{45}$$

Multiplying top and bottom by $I_pH^2(1 + as)$ gives

$$\frac{\theta_p}{T} = \frac{-1}{s^2I_p} \cdot \frac{[I_pH_3^2(1 + as) + s^2\{I_{11}I_{22}I_p(1 + kas) - I_{12}^2I_p(1 + ks)\}]}{[I_pH_3^2(1 + as) + s^2\{I_{22}(I_pI_{11} - I_{13}^2)(1 + kas) - (I_{12}^2I_p + I_{11}I_{23}^2 + 2I_{12}I_{13}I_{23})(1 + ks)\}]} \tag{46}$$

Thus, the denominator is now the same as for the ϕ/T case. Also, the numerator is of the same form as the denominator, and so may be factored in the same way as the denominator. Let

$$I_pH_3^2 = L' \qquad I_{11}I_{22}I_p = M' \qquad I_{12}^2I_p = N'$$

Then numerator factors are

$$L'\left[1 + \left(\frac{M'k - N' + a^2L'}{M' - N' + a^2L'}\right)as\right] \cdot \left[1 + \frac{aM'(1 - k)}{M' - N' + a^2L'}s + \frac{M' - N' + a^2kL'}{M' - N' + a^2L'} \cdot \frac{M' - N'}{L'}s^2\right]$$

The term $(M'k - N' + a^2L')/(M' - N' + a^2L')$ is very close to unity and so the numerator single real root can be cancelled with the denominator single root, (since slight differences in real roots would not produce any significant differences in the response).

The additional product introduced to the s^2 term is $(M' - N' + a^2kL')/(M' - N' + a^2L')$. This term is again closer to unity than 0.998, but it cannot be discounted for this reason, because it defines the position of the break frequency, and since the denominator break frequency is approximately the same value, the effect of using 1.0 instead of 0.998 could produce appreciable gain and phase errors at the small values of damping that are involved.

However, the ratio of the numerator s^2 correction factor $(M' - N' + a^2kL')/(M' - N' + a^2L')$ to the denominator s^2 correction factor, $(M - N + a^2kL)/(M - N + a^2L)$ is closer to unity than 1.000004 for the ITOS-1 spacecraft, and would be even closer for spacecraft in which the control axes

Table 1 Typical parameters examined for the ITOS-1 spacecraft

$I_{11} = 969$, $I_{22} = 839$, $I_{33} = 887$, $I_{12} = -9$,
$I_{23} = 0$, $I_{13} = 30$–90, $I_f = 12.6$, $I_D = 1.63^a$
$\alpha = 0.363$ lb in./rad/sec, $H = 200$ lb in. sec
Nutation frequency = 0.22 rads/sec
Uncoupled pitch loop gain and phase at nutation frequency = -6.91 *dB* and $-134.1°$
Nutation damper time constant = 155 min

[a] Where moments and products of inertia are lb in. sec^2.

were more nearly principal axes. This difference is indeed trivial, even bearing in mind the low damping. Therefore, it can be assumed that

$$(M' - N' + a^2kL')/(M' - N' + a^2L') = (M - N + a^2kL)/(M - N + a^2L) = Q$$

Since the newly derived numerator s term is

$$\frac{aM'(1-k)}{M' - N' + a^2L'} = \frac{(I_D/\gamma)I_{11}I_{22}I_pI_D/I_{22}}{I_{11}I_{22}I_p - I_{12}^2I_p + (I_D^2/\gamma^2)I_pH_3^2} \simeq \frac{I_D^2I_{11}\gamma}{I_{11}I_{22}\gamma^2 + I_D^2H_3^2}$$

i.e., the same as the denominator term; then

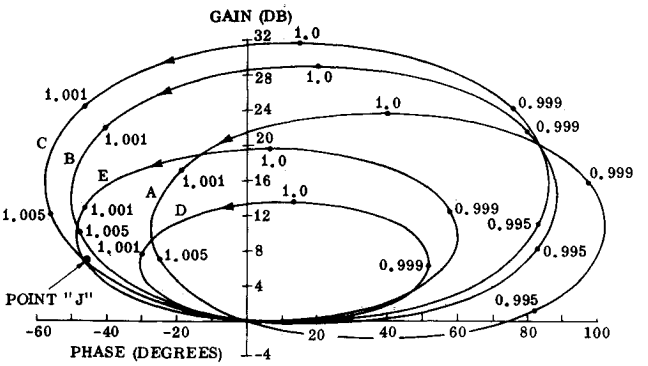

Fig. 7 Frequency plots of $f_c(s)$ (numbers on plots are values of normalized frequency ω/ω_N).

Thus, equating terms between the actual and simplified transfer functions, we obtain

$$T_D \cong \frac{(I_{11}I_{22})^{1/2}}{H_3} \qquad \zeta_D \cong \frac{I_D^2I_{11}\gamma H_3}{2(I_{11}I_{22}\gamma^2 + I_D^2H_3^2)} \cdot \frac{1}{(I_{11}I_{22})^{1/2}}$$

Therefore, fluid damper time constant

$$\tau_0 = (2I_{22}/\gamma)[1 + I_{11}I_{22}(\gamma/H_3I_D)^2]$$

$$\frac{\theta_p}{T} = \frac{-1}{s^2I_p} \cdot \frac{\{1 + (s/H_3)[I_D^2I_{11}\gamma H_3/(I_{11}I_{22}\gamma^2 + I_D^2H_3^2)] + (s^2/H_3^2)Q(I_{11}I_{22} - I_{12}^2)\}}{\{1 + (s/H_3)[(I_D^2I_{11}\gamma H_3)/(I_{11}I_{22}\gamma^2 + I_D^2H_3^2)] + Q\xi\}} \tag{47}$$

Thus since

$$\theta_E/T = \theta_p/T + d\beta/d\phi \cdot \phi/T$$

$$\frac{\theta_E}{T} = \frac{-1}{s^2I_p} \cdot \frac{\{1 + (s/H_3)[I_{13}d\beta/d\phi + I_D^2I_{11}\gamma H_3/(I_{11}I_{22}\gamma^2 + I_D^2H_3^2)] + (s^2/H_3^2)Q(I_{11}I_{22} - I_{12}^2) + (d\beta/d\phi)(I_{12}I_{13} + I_{11}I_{23})]\}}{\{1 + (s/H_3)[(I_D^2I_{11}\gamma H_3)/(I_{11}I_{22}\gamma^2 + I_D^2H_3^2)] + Q\xi\}} \tag{48}$$

Since Q is nearer to unity than 0.998 and also $(d\beta/d\phi)(I_{11}I_{23} + I_{12}I_{13})$ will generally be at least three orders smaller that $(I_{11}I_{22} - I_{12}^2)$, it will not introduce any significant error if the $(d\beta/d\phi)(I_{11}I_{23} + I_{12}I_{13})$ term in the numerator s^2 coefficient is multiplied by Q. The factor then becomes a product term with the numerator s^2 coefficient, as it is with the denominator s^2 coefficient. The effect of Q therefore is to move both numerator and denominator frequencies up or down slightly by the same ratio, and will not tend to pull the two frequencies apart. The Q term therefore has no appreciable effect and can thus be taken as unity in the above transfer function.

It will be remembered that the above derivation was based on a nutation damper on the roll axis. It can be shown that if the damper had been on the yaw axis, I_{11} would be replaced bI_{22} in the numerators of the two s coefficients.

Determination of the Nutation Decay Time Constant

The derived transfer function with fluid damper can be simplified as follows

$$\frac{\theta_E}{T} = \frac{1}{s^2I_p} \cdot \frac{1 + 2\zeta_NT_Ns + T_N^2s^2}{1 + 2\zeta_DT_Ds + T_D^2s^2} \tag{49}$$

where ζ_N, T_N, ζ_D, and T_D can be derived, if desired, by equating Eq. (48) to Eq. (49); $1/T_D$ is the natural frequency, or the nutation frequency and ζ_D is the nutation damping constant. Now the exponential decay time constant of the quadratic denominator, which must also be the nutation damper time constant is

$$\tau_0 = T_D/\zeta_D$$

Utilization of the Cross Coupled Transfer Function for Stability Analysis

In order to examine the stability of a closed-loop system, the over-all open-loop transfer function is required. Referring to Fig. 4, if the open-loop transfer function (T/θ_E) of the "Pitch Loop Control Hardware" is defined as $P(s)$, and the open-loop transfer function (θ_E/T) of the "Spacecraft Dynamics and Kinematics" is defined as $D(s)$, then the required open-loop system transfer function of the over-all pitch loop is $M(s) = P(s) \cdot D(s)$. It has been shown that $D(s)$ takes the form of Eq. (49) for the cross-coupled case, whereas if the cross-coupling were ignored, the equivalent single-axis (uncross-coupled) transfer function is, by Newton's laws:

$$D(s) = \theta_E/T = 1/s^2I_p \tag{50}$$

Comparing Eqs. (49) and (50) shows that the effect of the cross coupling on the pitch loop is to introduce the extra term $(1 + 2\zeta_NT_Ns + T_N^2s^2)/(1 + 2\zeta_DT_Ds + T_D^2s^2) = f_c(s)$ into the uncoupled open-pitch loop transfer function $M(s)$. Thus, if the frequency response of $M(s)$ is plotted on a Nichol's chart, it is only necessary to add the gain (in decibels) and the phase of $f_c(s)$ to this plot in order to determine the stability of the cross-coupled system.

However, because of the closeness of T_N to T_D and the very low damping inherent in both the numerator and denominator, the only frequencies at which the gain and phase of $f_c(s)$ are measurably different from 0 *dB* and 0° are in the vicinity of nutation frequency. For example, within the operational range of ITOS-1, the gain is within 1 *dB*, and the phase within 5° of zero for all frequencies greater or less than ±10%

of the nutation frequency. Within the range of $\pm 10\%$ of nutation frequency, large changes of gain and phase can occur in $f_c(s)$, depending upon the parameter values within it.

For all practical purposes therefore, the frequency response of $f_c(s)$ can be represented in a narrow frequency region in which the response of $M(s)$ virtually does not change. The cross-coupled Nichols plot can therefore be approximated very closely, by adding the response curve of $f_c(s)$ to the gain and phase point of $M(s)$ at nutation frequency only. Figure 5 illustrates this more clearly. In Fig. 5a is plotted typical gain vs phase responses of both $M(s)$ and $f_c(s)$. The gain and phase of $M(s)$ at nutation frequency is shown as G_N and $(\phi_N - 180)°$. Also, the phase margin of the uncoupled pitch loop $M(s)$, is shown as ϕ_p. Figure 5b shows how the $f_c(s)$ response is added to the curve of $M(s)$ at nutation frequency, thus producing the over-all cross-coupled response. This figure depicts how the phase margin has been reduced from ϕ_p to ϕ_M. A more direct way of obtaining the phase margin ϕ_M is illustrated in Fig. 5c. Here a simple shift of axes has been performed, such that the new axes origin passes through the gain and phase point of $M(s)$ at nutation frequency. Thus, $f_c(s)$ can be plotted directly on these new axes and the old stability point of 0 dB and 180° appears in the new axes system as point J. The coordinates of J are obviously $-G_N$ and $-\phi_N$. By comparing Figs. 5b and 5c, it can be seen that the measurement of the cross-coupled phase margin ϕ_M is the same in both cases.

This latter method was that used for the ITOS-1 studies, and it has several advantages. These are: 1) In order to assess the cross-coupled stability, the phase and gain of the control loop is only required at one frequency (nutation frequency). 2) The worst-case tolerances on parameters in the control loop are easily assessed, as those which change the phase and gain of point J in Fig. 5c to move it closest to the plot of $f_c(s)$. A simple analysis of the control-loop parameters will indicate this. 3) Conversely, the worst-case tolerances on parameters in the dynamics are those which move the plot of $f_c(s)$ closest to point J. In order to establish this criterion either of two approaches could be used: a) Frequency responses of $f_c(s)$ with the normalized terms ζ_D, ζ_N, T_N, T_D could show the stability as a function of these parameters. Worst-case conditions of the constituent parameters could then be established by relating them back to the normalized terms. b) Frequency responses of $f_c(s)$ could be derived, varying each parameter in turn to determine the worst cases.

The first of these two approaches gives good insight into the relative importance of the various elements in the transfer function, while the second gives a more absolute indication of stability. Both approaches are therefore useful. The second approach however, would require considerable calculation if the operation were to be performed by hand. Thus for the ITOS-1 study, the transfer function was programed on a time-sharing computer, to accept the spacecraft parameters and to print out a frequency response.

One point to note is that the tolerance on I_{11}, I_{22} and I_{33} will strongly affect point J, as well as $f_c(s)$, because changes in I_{11} and I_{22} shift the nutation frequency and changes in I_{33} are likely to change the control loop gain. Therefore, when establishing worst case conditions for these parameters, the effects of both $f_c(s)$ and point J should be considered simultaneously. A further point of interest is that for large negative values of $d\beta/d\phi$, ζ_N becomes negative. For such a case, the plot of $f_c(s)$ would not be a closed loop as shown in Fig. 5, but becomes an open line stretching from 0° to −360°. However, it has been shown that this line can also be considered to have occurred at one frequency, as it was for the closed loop, and that provided the Nyquist stability criterion is obeyed, stability can still be assessed for this case by the technique just described.

With the above described technique, the worst case conditions and stability boundaries were tentatively established for the ITOS-1 spacecraft. Then, using the results as a guide, a program of runs was made with the nonlinear hybrid simulation referred to in the introduction. It was then shown that a qualitative correspondence existed between the reciprocal of the closed-loop nutation damping time constant obtained from these runs and the equivalent phase margins obtained from the linear analysis. It was also shown that the nutation grew rather than decayed (negative reciprocal time constant) at all times when the phase margin was negative.

To illustrate this correlation, some typical results are presented. Figure 6 shows the reciprocal time constant, $1/\tau$ plotted against the sensor scan angle α, for two different values of I_{13}. All other parameters were as shown in Table I. As described in the "Description of System" and "Linearization of the Dynamic Equations" sections, α contributes to the cross-coupling by modifying the constant value assumed for $d\beta/d\phi$. For comparison purposes, the reciprocal time constant of the nutation damper, operating in the open-loop mode is shown as a broken line. The figure shows the rather surprising result that the larger value of I_{13} generally exhibits the better stability. It also shows that, over the range examined, stability is continually degraded as α is increased. Each point plotted on the curves was derived from hybrid computer time response, and the five points on Fig. 6 are reexamined on the linearized basis in Fig. 7. For clarity, the five points on Fig. 6 are labeled A–E with corresponding labeling of the $f_c(s)$ plots in Fig. 7. Also on Fig. 7, the servo phase and gain at nutation frequency is plotted as point J, in the manner described in the preceding section.

Comparing the reciprocal time constants of Fig. 6 with the phase margins in Fig. 7 illustrates the correlation that has earlier been described. By changing α, to move from curve A to curve B, the phase margin drops from about 20° to only 4°, which corresponds to the drop in reciprocal time constant in Fig. 6. Both figures indicate that although there is only a small margin, the system is still stable at B. However, when α is increased to point C in Fig. 6, the reciprocal time constant has become negative and the phase margin has also become negative by about 1°. This comparison of B with C indicates that the phase margin criterion for absolute stability is accurate to within a few degrees. The plots for D and E of Fig. 7 show the same trends of stability exhibited by Fig. 6. Also, by comparing plot A with D and B with E, in Fig. 7, confirmation is obtained that the largest I_{13} at a given α produces the most stable case. Also the unstable point E is again predicted by curve E with a negative phase margin of about one degree.

One of the qualitative uses of the linear method is also well illustrated in Fig. 7. If it is desired to stabilize the system under (say) condition C, by means of adjusting the closed control-loop gain, the figure shows that point J must be moved downwards. Moving point J downwards implies a gain increase in the control loop, a fact that would not have been expected or readily understood without the use of this technique. This latter phenomena has since been confirmed by the hybrid computer, wherein a reciprocal time constant increase was obtained when the control-loop gain was increased. Also the accuracy demonstrated in these examples, with which the transfer function can predict stability has been similarly proven by the hybrid computer for variations in momentum, damper, control loop and the other inertia parameters.

Conclusion

The transfer function and method of utilization described herein has been proven to be a very useful design tool; both by giving an insight into destabilizing parametric

trends, which therefore allows worst case conditions to be established, and also by showing quite accurately whether a given system will or will not be absolutely stable under these worst conditions. It should be remembered however, that the transfer function is based on small angles and perturbations. For any system where this is not the case, the quantitative merit of the transfer function should be reassessed by a comparison between its predictions and certain selected critical runs made on a full nonlinear computer simulation. Based on the results of the ITOS-1 spacecraft studies, various design changes were made to the control loop, pitch sensing equipment and inertia distribution, in order to optimize the stability boundaries under its various modes of operation. The in-orbit performance of the spacecraft now gives further verification of the method, and hence of its value as a design tool for dual-spin spacecraft.

References

[1] Landon, V. D. and Steward, B., "Nutational Stability of an Axisymmetric Body Containing a Rotor," *Journal of Spacecraft and Rockets*, Vol. 1, No. 6, June 1964, pp. 682–684.

[2] Likens, P. W., Tseng, G., and Mingori, D. L., "Stable Limit Cycles Due to Nonlinear Damping in Dual-Spin Spacecraft," *Journal of Spacecraft and Rockets*, Vol. 8, No. 6, June 1971, pp. 561–574.

[3] Likens, P. W., "Attitude Stability Criteria for Dual-Spin Spacecraft," *Journal of Spacecraft and Rockets*, Vol. 4, No. 2, Dec. 1967, pp. 1638–1643.

SEPTEMBER 1971 J. SPACECRAFT VOL. 8, NO. 9

Bearing Axis Wobble for a Dual Spin Vehicle

J. E. McIntyre* and M. J. Gianelli†
Hughes Aircraft Company, El Segundo, Calif.

Analytical expressions for the wobble motion of the bearing axis of a dual spin vehicle are derived in terms of the rotor static and dynamic unbalance. In the general case of arbitrary platform mass geometry, the bearing axis locus approximates a right cone with elliptical cross section. If the platform is configured so that the vehicle has equal transverse inertias in the platform fixed-coordinate system, the locus becomes circular and the wobble motion reduces to the familiar constant coning at spin speed which is encountered on single spin vehicles. Upper bounds on the mean and variance of the wobble angle are developed in terms of the statistical properties of the balancing process. The application of these bounds are indicated in an example problem which includes bearing run-out, ballast deployment uncertainty, propellant tank misalignment, bearing axis tilt and offset, and balancing machine static and dynamic residuals.

Nomenclature

$\mathbf{I}_1$ = rotor inertia matrix about rotor c.g.
$\mathbf{I}_2$ = platform inertia matrix about platform c.g.
Ω = relative rate of rotor with respect to platform
$\mathbf{r}_1$ = vector from system c.g. to rotor c.g.
$\mathbf{r}_2$ = vector from system c.g. to platform c.g.
m_1, m_2 = rotor and platform mass, respectively
$\mathbf{n}$ = unit vector along bearing axis
$\mathbf{r}$ = $\mathbf{r}_2 - \mathbf{r}_1$
m = reduced mass, $m_1m_2/(m_1 + m_2)$
$\boldsymbol{\epsilon}$ = rotor c.g. offset (normal to bearing axis)
$\epsilon_{x1}, \epsilon_{y1}$ = components of $\boldsymbol{\epsilon}$ in rotor coordinate system
$\boldsymbol{\delta}$ = rotor principal axis misalignment with respect to bearing axis
δ_{x1}, δ_{x2} = components of $\boldsymbol{\delta}$ in rotor coordinate system
z_0 = distance along bearing axis between platform and rotor c.g.
$\mathbf{h}$ = system angular momentum vector
$\boldsymbol{\omega}_1$ = angular rate of rotation of the rotor
$\boldsymbol{\omega}_2$ = angular rate of rotation of the platform
C_2 = symmetric platform axial inertia
$\mathbf{I}_3$ = $\mathbf{m}(\mathbf{r}\cdot\mathbf{r} - \mathbf{r}\mathbf{r}^T)$
$\mathbf{J}$ = $\mathbf{I}_1 + \mathbf{I}_2 + \mathbf{I}_3 - C_2\mathbf{n}\mathbf{n}^T$
C_1 = rotor axial inertia
A_1 = rotor transverse inertia about rotor c.g.
A_2 = symmetric platform transverse inertia about platform c.g.
$I_{x1z1} = (C_1 - A_1)\delta_{y1} - m\epsilon_{x1}z_0$; $I_{y1z1} = (A_1 - C_1)\delta_{x1} - m\epsilon_{y1}z_0$ } rotor cross products of inertia about system c.g.
$\boldsymbol{\theta}$ = angular vector denoting orientation of $\mathbf{h}$ vector with respect to bearing axis
A = $A_1 + A_2 + mz_0^2$ in symmetric platform case; $A_1 + (I_{x2x2} + I_{y2y2})/2$ in nonsymmetric case
ΔA = $(I_{x2x2} - I_{y2y2})/2$
$\mathbf{r}_0$ = vector from platform c.g. to the intersection of the bearing axis with the rotor c.g. plane
$\mathbf{I}_4 = \mathbf{I}_2 + m[\mathbf{r}_0\cdot\mathbf{r}_0 - \mathbf{r}_0\mathbf{r}_0^T] = \begin{pmatrix} I_{x2x2} & 0 & I_{x2z2} \\ 0 & I_{y2y2} & I_{y2z2} \\ I_{x2z2} & I_{y2y2} & I_{z2z2} \end{pmatrix}$
$\dot{\phi}$ = Ω
$c\phi, s\phi$ = $\cos\phi$, $\sin\phi$
$|A_0 - C_1|_{\text{MIN}}$ = MINIMUM $\{|A + \Delta A - C_1|, |A - \Delta A - C_1|\}$
E = expectation operator
$\boldsymbol{\beta}$ = vector denoting angular tilt of bearing axis with respect to balancing machine spindle axis
β_x, β_y = transverse components of $\boldsymbol{\beta}$
$\boldsymbol{\alpha}$ = vector from spindle axis to bearing axis in the alignment plane of the balancing machine
l = distance from alignment plane to rotor c.g.

Received December 10, 1970; revision received May 18, 1971.
Index categories: Spacecraft Attitude Dynamics and Control; Spacecraft Configurational and Structural Design.

* Senior Staff Engineer, Guidance and Dynamics Department. Member AIAA.
† Member of the Technical Staff, Guidance and Dynamics Department.

Introduction

In the past few years many papers and reports have appeared dealing with the nutational stability and control of dual spin vehicles.[1–5] A problem area of equal importance, as far as vehicle performances is concerned, is bearing axis